JOURNAL OF GUIDANCE, CONTROL, AND DYNAMICS
Vol. 25, No. 5, September–October 2002

Optimal Coordinated Maneuvers for Three-Dimensional Aircraft Conflict Resolution

Jianghai Hu*
University of California, Berkeley, Berkeley, California 94720-1772
Maria Prandini†
University of Brescia, 25123 Brescia, Italy
and
Shankar Sastry‡
University of California, Berkeley, Berkeley, California 94720-1772

The problem of designing optimal conflict-free maneuvers for multiple aircraft encounters is studied. The candidate maneuvers may involve changes not only of heading and speed but also of altitude. The goal is to determine, among all of the conflict-free maneuvers, the one that minimizes a certain energy cost function. A priority mechanism is incorporated into the energy function so that optimal resolution maneuvers are such that aircraft with lower priorities assume more responsibility in resolving the conflicts. Moreover, vertical maneuvers are penalized with respect to horizontal ones for the sake of passenger comfort. A geometric construction and a numerical algorithm for computing the optimal resolution maneuvers are given in the two-aircraft case. As for the multiple-aircraft case, an approximation scheme is proposed to compute a suboptimal two-legged solution. Extensive simulation results are presented to illustrate the effectiveness of the proposed algorithms.

Introduction

THE main concern of air traffic management (ATM) systems is guaranteeing safety. This is achieved by avoiding the occurrence of conflicts, that is, those situations where two aircraft come closer to each other than a minimum allowed horizontal separation R and a minimum allowed vertical separation H at the same time. Currently, R is set equal to 5 n mile (9.26 km) in en route airspace, and 3 n mile (5.556 km) inside the Terminal Radar Approach Control facilities (TRACONs), whereas H is 2000 ft (0.6096 km) above the altitude of 29,000 ft (8.8392 km, or FL 290), and 1000 ft (0.3048 km) below FL290. Conflict avoidance is typically decomposed into two phases:

1) The first phase is conflict detection, where potential conflicts that may arise in the future are detected by predicting the aircraft future motions based on the available information on their current positions, headings, and flight plans.

2) The second phase is conflict resolution, where the flight plans of the aircraft involved in the detected conflicts are replanned to prevent the conflicts from actually occurring.

In this paper we shall focus on conflict resolution. The existing approaches to aircraft conflict resolution can be classified according to various criteria. The interested reader is referred to the up-to-date survey[1] on the different conflict resolution approaches proposed in the literature. In the following, we shall review briefly some of the most relevant ones.

Based on the level of coordination or, alternatively, on the level of mutual trust among participating aircraft, conflict resolution methods can be classified as noncooperative and cooperative.[2]

In the noncooperative case, the aircraft involved in the encounter do not exchange information on their intentions and do not trust one another at all; hence, the worst-case approach is adopted. In the solution proposed in Refs. 3 and 4, the two-aircraft conflict resolution problem is formulated as each aircraft playing a zero-sum, noncooperative game against disturbances that model the uncertainty in the other aircraft's intentions, with the value function being the aircraft separation. The differential game methodology is also used in Ref. 5 for determining the safe region for aircraft approaching closely spaced parallel runways.

At the other extreme with respect to the noncooperative case, there is the cooperative conflict resolution scenario, where the current positions and intentions of the aircraft are assumed to be perfectly known to a supervising central controller. Each aircraft completely trusts the central controller (and, hence, all of the other aircraft), and is ready to follow its advice. The cooperative conflict resolution problem is typically formulated as an optimization problem, where the central controller designs the flight plans of all of the aircraft to avoid conflicts and at the same time minimize a certain cost function. Contributions in the literature belonging to this class include Refs. 6–10, to mention only a few.

In between the extremes of noncooperative and cooperative conflict resolution there are the probabilistic conflict resolution approaches. In these approaches, the aircraft positions are assumed to be distributed according to certain probabilistic laws, thus modeling not only the effect of disturbances on aircraft motions, but also that each aircraft has only partial confidence in the information on the intentions of other aircraft. References in this category include, for example, Refs. 11 and 12 for the two-aircraft case and Refs. 13 and 14 for the multiple-aircraft case.

Based on whether vertical maneuvers are employed or not, conflict resolution methods can be classified as three-dimensional or two-dimensional, with the latter being a particular case of the former. Typically, conflicts are resolved by resorting to three different kinds of aircraft actions (or any combination of them), turn, climb/descend, and accelerate/decelerate, that affect the aircraft heading, altitude, and speed, respectively. Resolution strategies adopting one or more of these actions are analyzed and compared in terms of cost and efficacy.[15] It is found that climb/descend is the most efficient action for resolving short-term conflicts because the horizontal separation requirement is much more stringent than the vertical one. In fact, vertical maneuvers are used to resolve imminent conflicts in the Traffic Alert and Collision Avoidance

Received 19 April 2001; revision received 17 December 2001; accepted for publication 7 March 2002. Copyright © 2002 by the American Institute of Aeronautics and Astronautics, Inc. All rights reserved. Copies of this paper may be made for personal or internal use, on condition that the copier pay the $10.00 per-copy fee to the Copyright Clearance Center, Inc., 222 Rosewood Drive, Danvers, MA 01923; include the code 0731-5090/02 $10.00 in correspondence with the CCC.

*Graduate Student, Department of Electrical Engineering and Computer Sciences, 211 Cory Hall No. 1772; jianghai@eecs.berkeley.edu. Student Member AIAA.

†Research Assistant, Department of Electronics for Automation, Via Branze 38; prandini@ing.unibs.it.

‡Professor, Department of Electrical Engineering and Computer Sciences, 269M Cory Hall; sastry@eecs.berkeley.edu.

System (TCAS)[16,17] currently operating onboard all commercial aircraft carrying more than 30 passengers. However, compared with horizontal maneuvers, excessive changes of altitude are likely to cause more discomfort to passengers and are not as compatible with the current vertically layered structure of the airspace. These issues, together with the relative simplicity of dealing with the two-dimensional case, have caused most of the approaches proposed in the literature to focus on two-dimensional conflict resolution, assuming level flight and horizontal resolution maneuvers.

In this paper, we address the problem of optimal cooperative three-dimensional conflict resolution involving multiple aircraft. Conflict situations involving more than two aircraft may actually occur in areas with high traffic density, and resolving them is intrinsically more difficult than dealing with the two-aircraft case. For example, it may happen that by solving a two-aircraft conflict without taking into consideration the surrounding aircraft, a new conflict with a third aircraft is generated (domino effect). Nevertheless, only a few of the existing treatments on conflict resolution deal with the multiple-aircraft case. Some of them[13,14,18] use the potential and vortex field method to determine coordinated maneuvers. However, the maneuvers thus generated are not guaranteed to be safe. Another approach consists in formulating multiple-aircraft conflict resolution as a constrained optimization problem with a suitable cost function to be optimized under the conflict-free constraint. The contributions belonging to this category[6–9,19–21] differ in the choice of model and cost function and also in the computational method adopted to solve the resultant optimization problem, for example, linear programming,[20] genetic algorithms,[6] semidefinite programming combined with a branch-and-bound search,[7] and sequential quadratic programming using linear approximation of the feasible region.[9] The last method is the closest in spirit to the approximation scheme we shall introduce in this paper, though we use a different formulation of the problem. In Ref. 19, the time-optimal cooperative conflict resolution maneuvers for multiple aircraft are studied using optimal control techniques. Solutions using computational geometric approaches are presented in Refs. 22–24.

This paper is organized as follows. First, we formulate precisely the optimal conflict resolution problem by proposing an energy cost function to select, among all of the conflict-free coordinated maneuvers, the optimal ones. By the use of this cost function, resolution maneuvers of not only shorter travel distance, but also less speed variation, are automatically favored, thus taking into account practical factors such as fuel consumption and passenger comfort, which are important in the ATM context. The energy cost function depends on some parameters that are introduced to assign different priorities to the aircraft, as well as to penalize vertical maneuvers.

Next, some necessary conditions for a conflict-free coordinated maneuver to be optimal are derived through a variational analysis. Compared with conventional variational problems, special attention has to be paid to the presence of the conflict-free constraint. We show that in the two-aircraft case the derived necessary conditions are sufficient to give a geometric characterization of the optimal resolution maneuvers. A numerical procedure is proposed to compute them, and simulation results for two-aircraft encounters are presented.

For the multiple-aircraft case, the original constrained optimization problem is approximated by a finite dimensional convex optimization problem with linear constraints. This is achieved by considering two-legged joint maneuvers specified by a set of waypoints and by linearly approximating the region to which the waypoints should belong for the corresponding two-legged joint maneuver to be conflict free. We describe how a not too conservative inner approximation scheme can be carried out and discuss the effect of various parameters on the optimal resolution maneuvers through simulation results.

The proposed approach presents some limitations. Specifically, constraints on the aircraft dynamics are not taken into account, and the adopted kinematic model is simplified. However, we discuss some methods that can be adopted to alleviate these limitations. In particular, we introduce additional (convex) constraints to restrict the sharp turns near the waypoints that would make the two-legged maneuvers not flyable in practice. Some conclusions are given at the end of the paper.

To aid the comprehension of the technical derivations, we attempt to stress the geometric interpretation of the obtained results wherever possible. Also, special attention is paid to the implementation issues of the proposed algorithms. The numerical accuracy of these algorithms is closely related to the software used for their implementations.

Problem Formulation

Consider a single aircraft i, flying from position $a_i \in \mathbb{R}^3$ at time t_0 to position $b_i \in \mathbb{R}^3$ at time t_f. Set $T \triangleq [t_0, t_f]$, and denote with $\boldsymbol{P}_i$ the set of all maneuvers for aircraft i, where a maneuver for aircraft i is defined to be a continuous and piecewise C^1 map α_i from T to $\mathbb{R}^3$ satisfying $\alpha_i(t_0) = a_i$ and $\alpha_i(t_f) = b_i$. Note that here piecewise C^1 means that there is a finite subdivision of T such that the map α_i is continuously differentiable to the first order on each open subinterval. In the following, $\dot{\alpha}_i(t)$ denotes the first derivative of α_i at those t where it is well defined, that is, at all except a finite number of $t \in T$.

The energy of a maneuver $\alpha_i : T \to \mathbb{R}^3$ is defined as

$$J(\alpha_i) = \frac{1}{2} \int_{t_0}^{t_f} \|\dot{\alpha}_i(t)\|^2 \, \mathrm{d}t \tag{1}$$

which can be interpreted as the integral of the instantaneous kinetic energy of a unit point mass whose motion is specified by α_i. Denote with $L(\alpha_i)$ the length of the curve α_i, that is,

$$L(\alpha_i) = \int_{t_0}^{t_f} \|\dot{\alpha}_i(t)\| \, \mathrm{d}t$$

Then, by the Cauchy–Schwartz inequality (see Ref. 25), $J(\alpha_i)$ satisfies

$$J(\alpha_i) \geq \frac{1}{2} \frac{L(\alpha_i)^2}{(t_f - t_0)}$$

The equality holds if and only if the speed $\|\dot{\alpha}_i(t)\|$ is constant, and in this case, the energy $J(\alpha_i)$ is proportional to the square of the length of α_i. This implies that the maneuver with the least energy for a single aircraft is the constant-speed motion along the line segment from its starting to its destination position. If the aircraft is forced to move along some fixed curve other than the line segment, then the parameterization of the curve with the least energy is the one with constant speed, and the minimal energy is proportional to the square of the curve length. As a result, the least energy maneuver between two points in the presence of static obstacles is the shortest curve joining the two points without passing through the obstacles parameterized proportionally to its arc length. This observation will be used in later sections when dealing with the two-aircraft case.

In the following development, we assume that a group of aircraft flying in a certain region of airspace have been isolated so that only conflicts among aircraft in this group need to be considered during the time interval of interest. This assumption, although impractical, is commonly adopted in the literature on conflict resolution.

Suppose that there are n aircraft in the group and they are numbered from 1 to n. Each aircraft i starts from position $a_i \in \mathbb{R}^3$ at time t_0 and arrives at position $b_i \in \mathbb{R}^3$ at time t_f, $i = 1, \ldots, n$. $\boldsymbol{P}_i$ is defined earlier. Set $\boldsymbol{P}(\boldsymbol{a}, \boldsymbol{b}) \triangleq \boldsymbol{P}_1 \times \cdots \times \boldsymbol{P}_n$, where $\boldsymbol{a} = (a_1, \ldots, a_n)$ and $\boldsymbol{b} = (b_1, \ldots, b_n)$ denote the starting and destination positions of the n-aircraft system, respectively. Each element $\alpha = (\alpha_1, \ldots, \alpha_n)$ of $\boldsymbol{P}(\boldsymbol{a}, \boldsymbol{b})$ is called a joint maneuver (n-maneuver, or simply a maneuver when there is no ambiguity) for the n-aircraft system. A joint maneuver $\alpha = (\alpha_1, \ldots, \alpha_n) \in \boldsymbol{P}(\boldsymbol{a}, \boldsymbol{b})$ is said to be conflict free if, for the duration of the encounter, none of the aircraft enters the cylindrical protection zone of radius R and height $2H$ surrounding another aircraft. If, for an arbitrary $c \in \mathbb{R}^3$, we denote by $c_{xy} \in \mathbb{R}^2$ and $c_z \in \mathbb{R}$ its components on the horizontal xy plane and the vertical z axis, respectively, then the conflict-free condition is equivalent to the condition that there is no pair of indices (i, j), $1 \leq i < j \leq n$, such that $\|\alpha_{i,xy}(t) - \alpha_{j,xy}(t)\| < R$ and $|\alpha_{i,z}(t) - \alpha_{j,z}(t)| < H$ for some $t \in T$.

We denote with $\boldsymbol{P}(R, H; \boldsymbol{a}, \boldsymbol{b})$ the set of all conflict-free (joint) maneuvers with starting position $\boldsymbol{a} = (a_1, \ldots, a_n)$ and destination position $\boldsymbol{b} = (b_1, \ldots, b_n)$ for the n-aircraft system. Conflict-free maneuvers will occasionally be called resolution maneuvers.

Throughout the paper we assume that each pair of points in the n-tuple $(a_1, \ldots, a_n)$ satisfies either the horizontal or the vertical separation condition so that there is no conflict for the n-aircraft system at time t_0, similarly for $(b_1, \ldots, b_n)$. As a result, the set $\boldsymbol{P}(R, H; \boldsymbol{a}, \boldsymbol{b})$ is nonempty.

The performance of each n-maneuver $\alpha \in \boldsymbol{P}(\boldsymbol{a}, \boldsymbol{b})$ can be characterized in terms of the cost function:

$$J_\mu(\alpha) \triangleq \sum_{i=1}^{n} \mu_i J(\alpha_i) \tag{2}$$

where $J(\alpha_i)$ is the energy of α_i defined in Eq. (1), and $\mu_1, \ldots, \mu_n$ are positive real numbers adding up to 1 that represent the priorities of the aircraft. Given a joint maneuver $\alpha \in \boldsymbol{P}(\boldsymbol{a}, \boldsymbol{b})$, we call $J_\mu(\alpha)$ its μ-energy. In the absence of the separation constraint, the μ-energy minimizing joint maneuver is clearly the one where each aircraft flies at constant speed along the straight line joining its starting to its destination position. If we consider the separation requirement, then the conflict-free maneuver with minimal μ-energy will still tend to be straight and smooth, and this has important practical implications in terms of, for example, fuel consumption and passenger comfort. By an appropriate choice of the coefficients $\mu_i, i = 1, \ldots, n$, one can assign different priorities to the n aircraft. In particular, one can associate smaller μ_i to those aircraft with higher maneuverability so that they will assume a larger responsibility in resolving the conflict.

Our goal is to solve the following constrained optimization problem:

$$\text{Minimize} \quad J_\mu(\alpha) \quad \text{subject to} \quad \alpha \in \boldsymbol{P}(R, H; \boldsymbol{a}, \boldsymbol{b}) \tag{3}$$

Each solution α^* to problem (3) is called an optimal (resolution) maneuver for the n-aircraft system.

In this formulation, it can be expected that the optimal resolution maneuvers will mainly utilize the vertical dimension for almost all encounters because the minimum allowed vertical distance H is much smaller than the minimum allowed horizontal distance R. However, vertical maneuvers are usually the least comfortable ones for passengers. This is the reason why we now redefine the energy of a maneuver α_i in Eq. (1) as follows:

$$J(\alpha_i) = \frac{1}{2} \int_{t_0}^{t_f} \left[\|\dot{\alpha}_{i,xy}(t)\|^2 + \eta^2 |\dot{\alpha}_{i,z}(t)|^2 \right] \mathrm{d}t \tag{4}$$

where $\eta \geq 1$ is a coefficient introduced to penalize the vertical maneuvers. The μ-energy of a joint maneuver α is then defined by Eq. (2) with $J(\alpha_i)$ given by Eq. (4) instead of by Eq. (1). Note that this modification does not add further difficulties to the solution of problem (3) because the minimization of the new cost function can be easily reduced to the earlier one without penalty by scaling the z axis by a factor of η. After the scaling, the starting and destination positions $\boldsymbol{a}$ and $\boldsymbol{b}$ of the n-aircraft system become $\boldsymbol{a}'$ and $\boldsymbol{b}'$, whereas the radius and the height of the protection zone become R and $2\eta H$, respectively. Each conflict-free maneuver $\alpha \in \boldsymbol{P}(R, H; \boldsymbol{a}, \boldsymbol{b})$ is scaled to a conflict-free maneuver α' in $\boldsymbol{P}(R, \eta H; \boldsymbol{a}', \boldsymbol{b}')$, and the μ-energy with penalty η of α is, in fact, equal to the μ-energy without penalty of α'. Therefore, optimal solutions to the original problem can be obtained by first minimizing $J_\mu(\alpha')$ subject to $\alpha' \in \boldsymbol{P}(R, \eta H; \boldsymbol{a}', \boldsymbol{b}')$ with no penalty on the vertical maneuvers, and then mapping the obtained solutions to $\boldsymbol{P}(R, H; \boldsymbol{a}, \boldsymbol{b})$ by scaling the z coordinates back by a factor of $1/\eta$.

Note that the protection zone of the scaled problem is a cylinder of radius R and height $2\eta H$. Hence, for larger η, horizontal resolution maneuvers are more likely to be invoked. In particular, in the level flight case, if $\eta \to \infty$ the problem degenerates into the two-dimensional resolution problem studied in Ref. 21.

Without loss of generality, we shall assume $\eta = 1$ in the following development.

μ-Alignment Condition

The starting and destination positions $\boldsymbol{a}$ and $\boldsymbol{b}$ of an n-aircraft system are said to be μ-aligned if they have the same μ-centroid, that is, if

$$\sum_{i=1}^{n} \mu_i a_i = \sum_{i=1}^{n} \mu_i b_i$$

In this section, we shall prove two necessary conditions for a conflict-free maneuver to be optimal. The first condition (Proposition 1) implies that it suffices to solve problem (3) for μ-aligned $\boldsymbol{a}$ and $\boldsymbol{b}$; the second condition (Proposition 2) states that the μ-centroid of an optimal solution to problem (3) moves at constant speed along the straight line from the μ-centroid of $\boldsymbol{a}$ to the μ-centroid of $\boldsymbol{b}$. These two conditions will be used in the next section to obtain the optimal resolution maneuvers for two-aircraft encounters.

For each $w \in \mathbb{R}^3$, we denote with $\boldsymbol{b} + w$ the n-tuple $(b_1 + w, \ldots, b_n + w)$, which can be thought of as a new destination position of the n-aircraft system.

Definition 1: The tilt operator $\mathcal{T}_w : \boldsymbol{P}(R, H; \boldsymbol{a}, \boldsymbol{b}) \to \boldsymbol{P}(R, H; \boldsymbol{a}, \boldsymbol{b} + w)$ is a map such that for any $\alpha \in \boldsymbol{P}(R, H; \boldsymbol{a}, \boldsymbol{b})$, $\beta = \mathcal{T}_w(\alpha) \in \boldsymbol{P}(R, H; \boldsymbol{a}, \boldsymbol{b} + w)$ is defined by $\beta_i(t) = \alpha_i(t) + [(t - t_0)/(t_f - t_0)]w, \forall t \in T, i = 1, \ldots, n$. It is easily verified that $\mathcal{T}_w \circ \mathcal{T}_{-w} = \mathcal{T}_{-w} \circ \mathcal{T}_w = \mathrm{id}$, where $\circ$ denotes map composition and id the identity map. Hence, $\mathcal{T}_w$ is a bijection.

Proposition 1: Suppose that $\alpha^* \in \boldsymbol{P}(R, H; \boldsymbol{a}, \boldsymbol{b})$ is an optimal solution to problem (3). Then $\beta^* = \mathcal{T}_w(\alpha^*)$ minimizes $J_\mu(\beta)$ subject to $\beta \in \boldsymbol{P}(R, H; \boldsymbol{a}, \boldsymbol{b} + w)$.

Proof: For any $\beta \in \boldsymbol{P}(R, H; \boldsymbol{a}, \boldsymbol{b} + w)$, let $\alpha = \mathcal{T}_{-w}(\beta)$. Then $\alpha \in \boldsymbol{P}(R, H; \boldsymbol{a}, \boldsymbol{b})$, and $J_\mu(\beta)$ can be expressed as

$$\begin{aligned} J_\mu(\beta) &= \frac{1}{2} \int_{t_0}^{t_f} \sum_{i=1}^{n} \mu_i \|\dot{\beta}_i(t)\|^2 \, \mathrm{d}t = \frac{1}{2} \int_{t_0}^{t_f} \sum_{i=1}^{n} \mu_i \left\| \dot{\alpha}_i(t) \right. \\ &\quad \left. + \frac{w}{t_f - t_0} \right\|^2 \mathrm{d}t = \frac{1}{2} \int_{t_0}^{t_f} \sum_{i=1}^{n} \mu_i \|\dot{\alpha}_i(t)\|^2 \, \mathrm{d}t \\ &\quad + \int_{t_0}^{t_f} \frac{w^T}{t_f - t_0} \sum_{i=1}^{n} \mu_i \dot{\alpha}_i(t) \, \mathrm{d}t + \frac{\|w\|^2}{2(t_f - t_0)} \\ &= J_\mu(\alpha) + \frac{w^T \left(\sum_{i=1}^{n} \mu_i (b_i - a_i) + w/2 \right)}{t_f - t_0} \end{aligned} \tag{5}$$

Notice that the second term in the last expression is a constant independent of β. Denote it by C. From Eq. (5) and the optimality of α^*, it follows that $J_\mu(\beta) \geq J_\mu(\alpha^*) + C, \forall \beta \in \boldsymbol{P}(R, H; \boldsymbol{a}, \boldsymbol{b} + w)$, where equality holds if $\alpha = \alpha^*$ and, hence, if $\beta = \beta^*$. This concludes the proof. □

For arbitrary $\boldsymbol{a}$ and $\boldsymbol{b}$, set $\boldsymbol{b}' = \boldsymbol{b} + w$, where

$$w = \sum_{i=1}^{n} \mu_i (a_i - b_i)$$

then $\boldsymbol{a}$ and $\boldsymbol{b}'$ are μ-aligned. By Proposition 1, solving problem (3) for the μ-aligned $\boldsymbol{a}$ and $\boldsymbol{b}'$ is equivalent to solving problem (3) for the original $\boldsymbol{a}$ and $\boldsymbol{b}$. Therefore, there is no loss of generality if we focus in the sequel on the μ-aligned case.

We next introduce the drift operation on joint maneuvers, which has the property of generating a conflict-free maneuver when applied to a conflict-free maneuver. This operator is used in the proof of Proposition 2.

Definition 2: Let $\gamma : T \to \mathbb{R}^3$ be a continuous and piecewise C^1 map such that $\gamma(t_0) = \gamma(t_f) = 0$. Then the drift operator $\mathcal{D}_\gamma : \boldsymbol{P}(R, H; \boldsymbol{a}, \boldsymbol{b}) \to \boldsymbol{P}(R, H; \boldsymbol{a}, \boldsymbol{b})$ is a map such that for any $\alpha \in \boldsymbol{P}(R, H; \boldsymbol{a}, \boldsymbol{b})$, $\beta = \mathcal{D}_\gamma(\alpha) \in \boldsymbol{P}(R, H; \boldsymbol{a}, \boldsymbol{b})$ is defined by $\beta_i(t) = \alpha_i(t) + \gamma(t), \forall t \in T, i = 1, \ldots, n$.

Because the μ-energy of an optimal resolution maneuver can not decrease under the perturbation of any drift operation, one can derive the optimality condition in Proposition 2. The proof starts by considering the μ-aligned case and then proceeds to the case of arbitrary $\boldsymbol{a}$ and $\boldsymbol{b}$ by the use of the conclusion of Proposition 1.

Proposition 2: Assume that $\alpha^* \in \boldsymbol{P}(R, H; \boldsymbol{a}, \boldsymbol{b})$ is an optimal solution to problem (3). Then

$$\sum_{i=1}^{n} \mu_i \alpha_i^*(t) = \sum_{i=1}^{n} \mu_i a_i + \frac{t - t_0}{t_f - t_0} \left(\sum_{i=1}^{n} \mu_i b_i - \sum_{i=1}^{n} \mu_i a_i \right) \qquad \forall t \in T \quad (6)$$

which, in the case of μ-aligned $\boldsymbol{a}$ and $\boldsymbol{b}$, reduces to

$$\sum_{i=1}^{n} \mu_i \alpha_i^*(t) = \sum_{i=1}^{n} \mu_i a_i = \sum_{i=1}^{n} \mu_i b_i, \qquad \forall t \in T$$

Proof: We start by considering the case when $\boldsymbol{a}$ and $\boldsymbol{b}$ are μ-aligned. Consider a continuous and piecewise C^1 map $\gamma : T \to \mathbb{R}^3$ satisfying $\gamma(t_0) = \gamma(t_f) = 0$. For each $\lambda \in \mathbb{R}$ define $\beta_\lambda \triangleq \mathcal{D}_{\lambda\gamma}(\alpha^*)$. Note that $\beta_\lambda \in \boldsymbol{P}(R, H; \boldsymbol{a}, \boldsymbol{b})$ for all $\lambda \in \mathbb{R}$. Then

$$J_\mu(\beta_\lambda) - J_\mu(\alpha^*) = \frac{1}{2} \int_{t_0}^{t_f} \sum_{i=1}^{n} \mu_i \left\| \dot{\alpha}_i^*(t) + \lambda \dot{\gamma}(t) \right\|^2 \mathrm{d}t - J_\mu(\alpha^*)$$

$$= \frac{\lambda^2}{2} \int_{t_0}^{t_f} \|\dot{\gamma}(t)\|^2 \, \mathrm{d}t + \lambda \int_{t_0}^{t_f} \dot{\gamma}(t)^T \sum_{i=1}^{n} \mu_i \dot{\alpha}_i^*(t) \, \mathrm{d}t$$

The difference $J_\mu(\beta_\lambda) - J_\mu(\alpha^*)$ is a quadratic function of λ which, by the optimality of α^*, must be nonnegative for all $\lambda \in \mathbb{R}$. Hence,

$$\int_{t_0}^{t_f} \dot{\gamma}(t)^T \sum_{i=1}^{n} \mu_i \dot{\alpha}_i^*(t) \, \mathrm{d}t = 0$$

must hold for any choice of γ such that $\gamma(t_0) = \gamma(t_f) = 0$. Because $\boldsymbol{a}$ and $\boldsymbol{b}$ are μ-aligned, we can choose

$$\gamma(t) = \sum_{i=1}^{n} \mu_i \alpha_i^*(t) - \sum_{i=1}^{n} \mu_i a_i$$

Given that α^* is piecewise C^1, this leads to

$$\sum_{i=1}^{n} \mu_i \dot{\alpha}_i^*(t) = 0$$

for almost all $t \in T$, and hence, by integration, to the desired conclusion for the μ-aligned case.

For the general case when $\boldsymbol{a}$ and $\boldsymbol{b}$ are not necessarily μ-aligned, let

$$w = \sum_{i=1}^{n} \mu_i (a_i - b_i)$$

Then $\mathcal{T}_w$ maps α^* to $\beta^* = \mathcal{T}_w(\alpha^*)$, which, by Proposition 1, minimizes $J_\mu(\beta)$ over all $\beta \in \boldsymbol{P}(R, H; \boldsymbol{a}, \boldsymbol{b}')$ with $\boldsymbol{b}' = \boldsymbol{b} + w$. Because $\boldsymbol{a}$ and $\boldsymbol{b}'$ are μ-aligned, we know from the preceding that

$$\sum_{i=1}^{n} \mu_i \beta_i^*(t) = \sum_{i=1}^{n} \mu_i a_i, \qquad \forall t \in T$$

The desired conclusion (6) is then obtained by using the relation $\alpha^* = \mathcal{T}_{-w}(\beta^*)$. □

Optimal Maneuvers for Two-Aircraft Encounters

In this section we describe how optimal resolution maneuvers for two-aircraft encounters can be constructed. This construction will be used in the next section to determine an approximate solution to problem (3) in the multiple-aircraft case.

Assume that $\boldsymbol{a} = (a_1, a_2)$ and $\boldsymbol{b} = (b_1, b_2)$ are μ-aligned and denote with c their common μ-centroid, that is, $c = \mu_1 a_1 + \mu_2 a_2 = \mu_1 b_1 + \mu_2 b_2$. By Proposition 2, an optimal two-maneuver $\alpha^* = (\alpha_1^*, \alpha_2^*) \in \boldsymbol{P}(R, H; \boldsymbol{a}, \boldsymbol{b})$ satisfies

$$\alpha_1^*(t) - c = -\mu_2/\mu_1 (\alpha_2^*(t) - c), \qquad \forall t \in T \quad (7)$$

from which it easily follows that the energies of α_1^* and α_2^* are related by $\mu_1^2 J(\alpha_1^*) = \mu_2^2 J(\alpha_2^*)$. Hence, the problem becomes finding, among all conflict-free maneuvers satisfying Eq. (7), the one that minimizes the energy of the maneuver for a single aircraft, for example, aircraft 1. The separation constraint can be simplified as well because by Eq. (7) it is equivalent to the condition that the curve $\alpha_1^*(\cdot)$ never enters the open cylinder W_μ of radius $R_\mu = \mu_2 R$ and height $2H_\mu = 2\mu_2 H$ centered symmetrically around the μ-centroid c.

As a result of these simplifications, problem (3) is equivalent to

$$\text{minimize } J(\alpha_1) \text{ subject to } \alpha_1 \in \boldsymbol{P}_1, \text{ and } \alpha_1(t) \in \mathbb{R}^3 \backslash W_\mu \text{ for all } t \in T \quad (8)$$

which consists in finding minimum energy maneuvers of a single aircraft in the presence of the static obstacle W_μ. From the discussions following definition (1) of the energy of a maneuver, we then know that a solution to problem (8) is a constant-speed motion along a shortest curve joining a_1 to b_1 while avoiding the obstacle W_μ. Under the feasibility assumption, both a_1 and b_1 belong to $\mathbb{R}^3 \backslash W_\mu$, and such a curve can be computed efficiently by an algorithm given later. Once α_1^* is computed, α_2^* can be obtained from α_1^* through Eq. (7), thus concluding the discussions on the μ-aligned case.

For the general case when $\boldsymbol{a}$ and $\boldsymbol{b}$ are not necessarily μ-aligned, by Proposition 1, an optimal solution $\alpha^* \in \boldsymbol{P}(R, H; \boldsymbol{a}, \boldsymbol{b})$ to problem (3) is given by

$$\alpha_1^*(t) = \gamma_1^*(\boldsymbol{a}, \boldsymbol{b} + w)(t) - [(t - t_0)/(t_f - t_0)]w$$

$$\alpha_2^*(t) = \gamma_2^*(\boldsymbol{a}, \boldsymbol{b} + w)(t) - [(t - t_0)/(t_f - t_0)]w \qquad \forall t \in T \quad (9)$$

where $[\gamma_1^*(\boldsymbol{a}, \boldsymbol{b} + w), \gamma_2^*(\boldsymbol{a}, \boldsymbol{b} + w)]$ denotes an optimal conflict-free maneuver in $\boldsymbol{P}(R, H; \boldsymbol{a}, \boldsymbol{b} + w)$ with $w = \mu_1 a_1 - \mu_1 b_1 + \mu_2 a_2 - \mu_2 b_2$. (Note that $\boldsymbol{a}$ and $\boldsymbol{b} + w$ are μ-aligned.)

The optimal solutions depend on the choice of the priority coefficients μ_1 and μ_2. Consider the case when the priority of aircraft 1 is much larger than that of aircraft 2, so that $\mu_2 \simeq 0$. In the μ-aligned case, this implies that $a_1 \simeq b_1$, and the radius and height of the cylinder W_μ are approximately 0. Therefore, γ_1^* is nearly a zero motion. For general $\boldsymbol{a}$ and $\boldsymbol{b}$ that are not necessarily μ-aligned, it follows from the first equation in Eq. (9) that optimal maneuvers for aircraft 1 are almost the constant-speed motion along the line segment from a_1 to b_1. Hence, as expected, aircraft 1 behaves as if there were no other aircraft flying in the same region, whereas aircraft 2 is the one assuming the responsibility of avoiding conflicts.

Examples of Optimal Two-Maneuvers

In this section, we present some examples of two-aircraft encounters and discuss the influence of various factors on the corresponding optimal resolution maneuvers. In all of the examples, the coordinates of the aircraft positions are measured in nautical miles with $R = 5$ n mile (9.26 km) and $H = 0.3292$ n mile (0.6096 km).

We start by considering a two-aircraft encounter where $a_1 = (0, 20, 1)$, $b_1 = (40, 20, 1)$ and $a_2 = (20, 0, 1)$, $b_2 = (20, 40, 1)$, so that the two straight lines each connecting the starting and destination positions of an aircraft are on the same horizontal plane and cross each other at a right angle. These two lines are the ideal trajectories of the two aircraft.

Figure 1 shows an optimal maneuver in the case when the two aircraft have the same priority ($\mu_1 = \mu_2 = 0.5$) and $\eta = 5$. The starting and destination positions of the two aircraft are marked with stars and diamonds, respectively, whereas the circles represent the aircraft positions at equally spaced time instants. Hence, the denser the circles, the slower the motions. The top view in Fig. 1b shows that the conflict is resolved by vertical deviations from the ideal trajectories.

We now study the effect of the priority coefficients on the optimal resolution maneuvers. Plotted in Fig. 2 are optimal resolution maneuvers for the same two-aircraft orthogonal encounter under three different sets of aircraft priorities and the same $\eta (= 5)$. Although the optimal maneuvers in all three cases have the same top view (shown

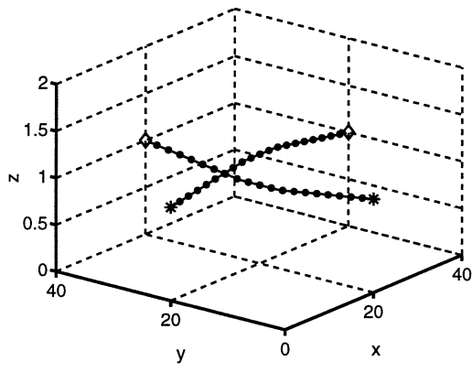

a) Three-dimensional representation

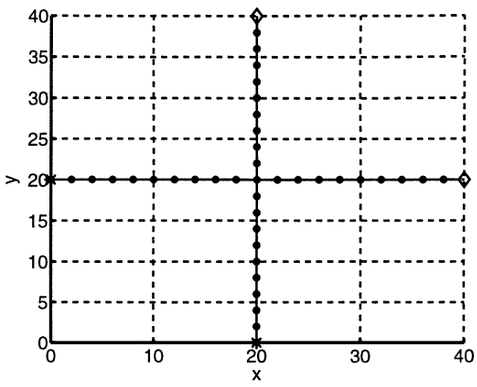

b) Top view

Fig. 1 Optimal resolution maneuver for an orthogonal two-aircraft encounter ($\eta = 5$ and $\mu_1 = \mu_2 = 0.5$).

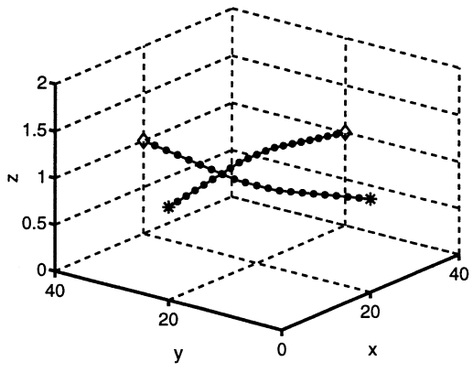

a) $\mu_1 = 0.5$, $\mu_2 = 0.5$

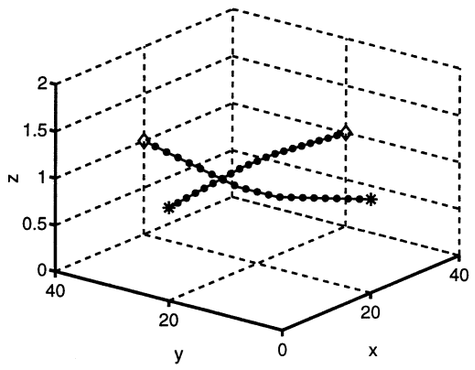

b) $\mu_1 = 0.7$, $\mu_2 = 0.3$

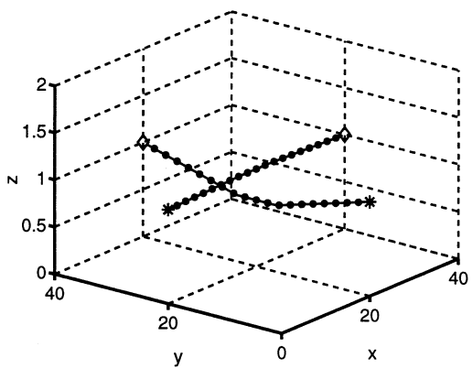

c) $\mu_1 = 0.9$, $\mu_2 = 0.1$

Fig. 2 Optimal resolution maneuvers for the orthogonal two-aircraft encounter under three different sets of aircraft priorities ($\eta = 5$).

in Fig. 1b), the vertical deviation of aircraft 1 from its ideal trajectory decreases as its priority increases. In other words, aircraft 2 with smaller priority will assume more responsibility in resolving the conflict. In the extreme case, when $\mu_1 = 1$ and $\mu_2 = 0$, the optimal resolution maneuver will be such that aircraft 1 flies along its ideal trajectory and aircraft 2 assumes all of the responsibility of avoiding conflicts with aircraft 1. These conclusions hold in general for multiple-aircraft encounters.

As for the effect of the vertical penalty factor, note that in Fig. 1, where $\eta = 5$ and $\mu_1 = \mu_2 = 0.5$, the conflict is resolved using only vertical deviations from the ideal trajectories. In contrast, in the case shown in Fig. 3, where η is set equal to $15(\mu_1 = \mu_2 = 0.5)$, the conflict is resolved using only horizontal deviations. The explanation is that, to obtain the optimal resolution maneuvers, we have to scale the z axis by a factor of η. When η is so large that the height of the cylindrical obstacle becomes much larger than its radius, a shortest curve between two points across the cylinder is more likely to be a curve around the side of the cylinder than around its top or bottom. Therefore, the larger the vertical penalty factor η, the more likely it is that an optimal resolution maneuver will consist of horizontal deviations from the ideal trajectories. In general, for encounters involving two or more aircraft, there are two extreme cases: When η is very large and the aircraft initial and destination positions are all at about the same altitude, the problem degenerates into a planar conflict resolution problem, where only horizontal deviations are allowed in resolving the conflict; when η is close to 0, then only vertical deviations are used in the optimal resolution maneuvers and their top views consist of straight line segments.

Shortest Curve Between Two Points in $\mathbb{R}^3$ Avoiding a Cylindrical Obstacle

In this section, we address the problem of computing a shortest curve in $\mathbb{R}^3$ connecting two points while avoiding a cylindrical obstacle. This is to complete the solution to problem (3) in the two-aircraft case, that is, problem (8).

Consider a cylinder of radius r and height $2h$ centered at the origin:

$$D = \{(x, y, z) \in \mathbb{R}^3 : x^2 + y^2 < r^2 \text{ and } |z| < h\}$$

Given two points a and b in $\mathbb{R}^3 \backslash D$, we wish to

$$\text{find a shortest curve in } \mathbb{R}^3 \backslash D \text{ connecting } a \text{ and } b \tag{10}$$

We require the curve to be continuous and piecewise C^1 so that its arc length is well defined.

Curves that are locally distance minimizing are called geodesics. A shortest curve between two points is necessarily a geodesic. In this sense, problem (10) is a special instance of the general problem of finding distance-minimizing geodesics in manifolds with a (nonsmooth) boundary. Determining shortest curves in the presence of geometric obstacles is a well-studied problem in computational geometry (see Refs. 26 and 27). Here we study a very special case.

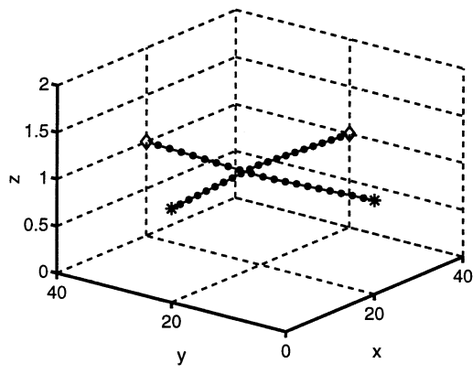

a) Three-dimensional representation

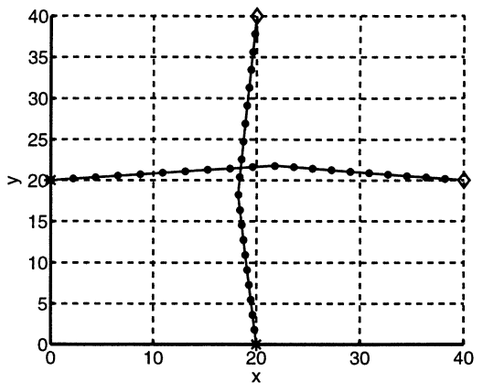

b) Top view

Fig. 3 Optimal resolution maneuver for the orthogonal two-aircraft encounter with larger $\eta = 15$ ($\mu_1 = \mu_2 = 0.5$).

It is obvious that, when a and b are visible to each other in the sense that the line segment joining a and b does not intersect the obstacle D, the shortest curve we are looking for is the straight line segment joining a and b; hence, the solution to problem (10) is trivial. Suppose now that a and b are not visible to each other.

Because the cylinder D is convex, a shortest curve in $\mathbb{R}^3 \backslash D$ connecting two points on its boundary ∂D is contained entirely in ∂D and is a distance-minimizing geodesic of ∂D in its own geometry. For general a and b not necessarily belonging to ∂D, we have Proposition 3.

Proposition 3: A shortest curve in $\mathbb{R}^3 \backslash D$ connecting a and b can be decomposed into three segments: a straight line segment from a to a point $p \in \partial D$, a geodesic segment of ∂D from p to a point $q \in \partial D$, and a straight line segment from q to b. Moreover, the two line segments are contained entirely in the interior of $\mathbb{R}^3 \backslash D$ except for their endpoints p and q.

If the shortest curve between a and b is viewed as a path traveled from a to b, then Proposition 3 says that the curve will enter and exit ∂D exactly once, at positions p and q, respectively. We then call p and q entry point and exit point, respectively. As a result of Proposition 3, solving problem (10) is equivalent to determining the entry point p, the exit point q, and the distance-minimizing geodesic segment on ∂D between p and q. In the case when $a \in \partial D$, $p = a$, and the first line segment degenerates into a single point. The case is similar for the second line segment if $b \in \partial D$. The middle geodesic segment in ∂D degenerates into a single point if $p = q$, in which case the two straight line segments are not collinear because a and b are assumed to be not visible to each other.

There are certain restrictions on the possible locations of p and q in ∂D. Denote with ∂D_T and ∂D_B the closed disks of radius r constituting, respectively, the top and bottom surfaces of the cylinder D. Denote with ∂D_S the side surface of D (boundary included). Then $\partial D = \partial D_T \cup \partial D_B \cup \partial D_S$. The entry point p and the exit point q must satisfy the following conditions. First of all, p is visible to a and q visible to b. Moreover, if a (respectively, b) is in the interior of $\mathbb{R}^3 \backslash D$, then p (respectively, q) belongs to the contour of D with respect to a viewer situated at a (respectively, b). In particular, this implies that $p \in \partial D_S$ unless a is in the interior of ∂D_T or ∂D_B, and $q \in \partial D_S$ unless b is in the interior of ∂D_T or ∂D_B.

Notice that D is a subset of the whole cylinder Q defined by $Q = \{(x, y, z) \in \mathbb{R}^3 : x^2 + y^2 < r^2\}$. We can then distinguish the following three cases:

1) Both a and b are outside of Q, and at least one of them has z coordinate in $[-h, h]$.

2) Both a and b are outside of Q, and neither of them has z coordinate in $[-h, h]$.

3) At least one of a and b belongs to Q.

In each one of these cases, solutions to problem (10) can assume only a finite number of possible configurations. We shall describe in the Appendix a numerical procedure to compute a shortest curve for each such configuration. Although, in general, it is difficult to obtain an analytic solution, one can reduce the problem to a finite number of simple optimization problems, each over a compact region of $\mathbb{R}^1$ or at most $\mathbb{R}^2$ and corresponding to an admissible configuration.

Optimal Two-Legged Maneuvers for Multiple-Aircraft Encounters

The approach adopted in the preceding sections cannot be easily generalized to the multiple-aircraft case because there are too many configurations to be considered. In this section, we simplify the problem by considering two-legged maneuvers specified by a set of waypoints.

Reformulation of the Problem

Consider an n-aircraft system with starting position $\boldsymbol{a} = (a_1, \ldots, a_n)$ and destination position $\boldsymbol{b} = (b_1, \ldots, b_n)$. Fix an epoch $t_c \in T$ such that $t_0 < t_c < t_f$. For each aircraft i, $i = 1, \ldots, n$, choose a waypoint $c_i \in \mathbb{R}^3$. A two-legged maneuver with waypoint c_i for aircraft i is a maneuver consisting of two stages: first from a_i at time t_0 to c_i at time t_c, and then from c_i at time t_c to b_i at time t_f, moving at constant velocity in both stages. Denote with $\boldsymbol{P}_{i,2}$ the set of all two-legged maneuvers of aircraft i, and with $\boldsymbol{P}_2(\boldsymbol{a}, \boldsymbol{b}) = \boldsymbol{P}_{1,2} \times \cdots \times \boldsymbol{P}_{n,2}$ the set of all two-legged joint maneuvers of the n-aircraft system. Denote with $\boldsymbol{P}_2(R, H; \boldsymbol{a}, \boldsymbol{b})$ the subset of $\boldsymbol{P}_2(\boldsymbol{a}, \boldsymbol{b})$ consisting of all those elements of $\boldsymbol{P}_2(\boldsymbol{a}, \boldsymbol{b})$ that are conflict free. We assume that the epoch t_c is fixed, so that each maneuver in $\boldsymbol{P}_2(\boldsymbol{a}, \boldsymbol{b})$ [and, hence, in $\boldsymbol{P}_2(R, H; \boldsymbol{a}, \boldsymbol{b})$] is uniquely specified by the waypoints $(c_1, \ldots, c_n)$. The choice of a uniform t_c for all of the aircraft is for the sake of simplicity. It is, in fact, possible to extend our approach to allow for different t_c for the aircraft, though at the cost of an increased problem complexity.

Now we try to solve the following problem:

$$\text{Minimize} \quad J_\mu(\alpha) \quad \text{subject to} \quad \alpha \in \boldsymbol{P}_2(R, H; \boldsymbol{a}, \boldsymbol{b}) \tag{11}$$

One reason why one should study problem (11) instead of the general problem (3) is due to the ATM practice: It is far simpler for the central controller to transmit the aircraft trajectory information in the form of waypoints and times to reach these waypoints rather than continuous trajectories. From a methodological point of view, because each maneuver in $\boldsymbol{P}_2(R, H; \boldsymbol{a}, \boldsymbol{b})$ is parameterized by a waypoints vector $(c_1, \ldots, c_n)$, which resides in a finite dimensional vector space, problem (11) is a finite dimensional optimization problem, which is much easier to deal with than the variational problem (3).

By using exactly the same arguments leading to Proposition 2, one can prove that the μ-alignment condition holds also for the two-legged case.

Proposition 4: Suppose that $(c_1^*, \ldots, c_n^*)$ are the waypoints of solution $\alpha^* \in \boldsymbol{P}_2(R, H; \boldsymbol{a}, \boldsymbol{b})$ to problem (11). Then,

$$\sum_{i=1}^{n} \mu_i c_i^* = \sum_{i=1}^{n} \mu_i a_i + \frac{t_c - t_0}{t_f - t_0} \left(\sum_{i=1}^{n} \mu_i b_i - \sum_{i=1}^{n} \mu_i a_i \right) \tag{12}$$

which, in the case of μ-aligned $\boldsymbol{a}$ and $\boldsymbol{b}$, reduces to

$$\sum_{i=1}^{n} \mu_i c_i^* = \sum_{i=1}^{n} \mu_i a_i = \sum_{i=1}^{n} \mu_i b_i$$

This condition is not sufficient for deriving the solutions to problem (11) when there are more than two aircraft involved. However, in the two-legged case, both the cost function and the constraints in problem (11) can be simplified, and a solution, though suboptimal in general, can be computed. We start by considering the cost function and discuss the constraints in a later section.

Let α be a two-legged joint maneuver in $\boldsymbol{P}_2(\boldsymbol{a}, \boldsymbol{b})$ with waypoints $(c_1, \ldots, c_n)$. Then α is specified by

$$\alpha_i(t) = \begin{cases} a_i + (c_i - a_i)[(t - t_0)/(t_c - t_0)], & t_0 \le t \le t_c \\ b_i + (c_i - b_i)[(t - t_f)/(t_c - t_f)], & t_c < t \le t_f \end{cases} \qquad i = 1, \ldots, n \quad (13)$$

It is easy to verify that the μ-energy of α (assuming $\eta = 1$) is given by

$$J_\mu(\alpha) = \frac{t_f - t_0}{(t_f - t_c)(t_c - t_0)} \sum_{i=1}^{n} \mu_i \left\| c_i - c_i^u \right\|^2 + C \qquad (14)$$

where C is a constant and

$$c_i^u = \frac{(t_f - t_c)a_i + (t_c - t_0)b_i}{t_f - t_0}, \qquad i = 1, \ldots, n \qquad (15)$$

are the optimal waypoints when minimizing $J_\mu(\alpha)$ without the conflict-free constraint. As a result of Eq. (14), problem (11) is equivalent to

$$\text{minimize} \quad \sum_{i=1}^{n} \mu_i \left\| c_i - c_i^u \right\|^2 \quad \text{subject to} \quad \alpha \in \boldsymbol{P}_2(R, H; \boldsymbol{a}, \boldsymbol{b}) \text{ with waypoints } (c_1, \ldots, c_n) \qquad (16)$$

where the cost function to be optimized is quadratic in the optimization variables $(c_1, \ldots, c_n)$.

Constraints on the Waypoints

The condition that the two-legged joint maneuver $\alpha \in \boldsymbol{P}_2(\boldsymbol{a}, \boldsymbol{b})$ with waypoints $(c_1, \ldots, c_n)$ is conflict free can be expressed in terms of constraints on $(c_1, \ldots, c_n)$. These constraints are, in general, nonconvex. We now study how they can be simplified and approximated by appropriate linear constraints.

Because $\alpha \in \boldsymbol{P}_2(R, H; \boldsymbol{a}, \boldsymbol{b})$ is equivalent to the condition that there is no conflict between any aircraft pair, we focus on aircraft 1 and 2 and temporarily ignore the presence of other aircraft.

Proposition 5: The condition that there is no conflict between aircraft 1 and aircraft 2 in $\alpha \in \boldsymbol{P}_2(\boldsymbol{a}, \boldsymbol{b})$ is equivalent to the condition that their waypoints c_1 and c_2 satisfy the following condition: $c_1 - c_2$ is visible to both $a_1 - a_2$ and $b_1 - b_2$ in $\mathbb{R}^3$ in the presence of the open cylindrical obstacle W of radius R and height $2H$ centered at the origin.

Proof: Notice that for any $w \in \mathbb{R}^3$ and $\alpha \in \boldsymbol{P}_2(\boldsymbol{a}, \boldsymbol{b})$, $\beta = \mathcal{T}_w(\alpha)$ is still a two-legged joint maneuver, though in $\boldsymbol{P}_2(\boldsymbol{a}, \boldsymbol{b} + w)$. Moreover, there is no conflict between aircraft 1 and 2 in β if and only if there is no conflict between aircraft 1 and 2 in α. We start by considering the first stage of the joint maneuver α. By choosing $w = [(t_f - t_0)/(t_c - t_0)](a_2 - c_2)$, the waypoint of aircraft 2 in maneuver β becomes a_2, and the waypoint of aircraft 1 becomes $a_2 + c_1 - c_2$. Thus, in the first stage of the motions specified by β, aircraft 2 stays at a_2, whereas aircraft 1 moves at constant velocity from a_1 to $a_2 + c_1 - c_2$. Therefore, the condition that there is no conflict between aircraft 1 and aircraft 2 during the first stage of the motions specified by β is equivalent to that the line segment from a_1 to $a_2 + c_1 - c_2$ does not intersect the cylinder of radius R and height $2H$ centered at a_2, or, equivalently, after a translation of $-a_2$, the line segment from $a_1 - a_2$ to $c_1 - c_2$ does not intersect W. Similar arguments can be applied to the second stage of the motions to show that there is no conflict between aircraft 1 and aircraft 2 during the second stage of the motions specified by α if and only if the line segment from $b_1 - b_2$ to $c_1 - c_2$ does not intersect W. □

Set $\Delta a = a_1 - a_2$, $\Delta b = b_1 - b_2$, and $\Delta c = c_1 - c_2$. By Proposition 5, the feasible region of Δc consists of those points in $\mathbb{R}^3$ visible to both Δa and Δb in the presence of the obstacle W. Such a region has a complex shape (in general, there is a hole in it). In particular, it is not convex. Hence, problem (16) is, in essence, a nonconvex optimization problem, which is not only difficult to solve, but may also admit multiple solutions. It is then natural to look for some convex approximation of the feasible region.

In safety-critical context such as in ATM systems, it is necessary that the approximation is strictly contained in the original feasible region to ensure absolute safety (inner approximation). On the other hand, the approximation should be as tight as possible so that the computed solutions are close to be optimal. The approximation scheme introduced below satisfies these requirements. Moreover, because it only uses the convexity of W, it can be easily generalized to the case when the protection zone has an arbitrary convex shape, not necessarily cylindrical.

In the following, we assume that both Δa and Δb belong to the interior of $\mathbb{R}^3 \backslash W$, which is satisfied in all situations in practice. We then distinguish two different cases depending on whether Δa and Δb are visible to each other in the presence of the obstacle W.

Δa and Δb Are Visible to Each Other

Suppose that the line segment joining Δa and Δb does not intersect W. In this case, there is no conflict between aircraft 1 and 2 if they both fly at constant speed along their ideal trajectories, which correspond to the two-legged joint maneuver with waypoints c_1^u and c_2^u defined in Eq. (15). Notice that $\Delta c^u = c_1^u - c_2^u$ is on the line segment between Δa and Δb and, hence, outside of W. From this it follows that the approximated feasible region of Δc should include Δc^u and as much region in $\mathbb{R}^3$ as possible, provided it is visible to both Δa and Δb. One such choice is described next.

Let L_{ab} be the line segment between Δa and Δb (endpoints included), and let $\bar{W}$ be the closure of W, which is a closed cylinder. Because both L_{ab} and $\bar{W}$ are compact and convex subsets of $\mathbb{R}^3$, there exists a point u in L_{ab} and a point v in W such that $\|u - v\| = \inf\{\|x - y\| : x \in L_{ab}, y \in \bar{W}\}$. If $u \neq v$, then through point v there is a unique plane P orthogonal to the straight line between u and v. P divides $\mathbb{R}^3$ into two closed half-spaces that intersect each other at P. The definition of u and v together with the convexity of L_{ab} and $\bar{W}$ implies that L_{ab} is contained in one half-space, whereas $\bar{W}$ is contained in the other half-space. We denote by P^+ the closed half-space containing L_{ab}. If $u = v$, then u (hence, v) is located on ∂W. In this case, we can choose any tangent plane to ∂W at u that separates L_{ab} and $\bar{W}$ and define P^+ to be the side of it containing L_{ab}. Note that here we use the term tangent planes of ∂W in its generalized sense, that is, those planes that intersect ∂W and have W on one side exclusively. In the special case when $u = v$ and u is on the sharp edges of ∂W, there might be a family of such tangent planes, and we can choose any one of them in defining P^+, provided it separates L_{ab} and $\bar{W}$.

The closed half-space P^+ thus obtained satisfies the condition that it contains Δc^u and that all of its points are visible to both Δa and Δb. Therefore, we can use P^+ as the approximated feasible region of Δc. This, in essence, imposes a single linear constraint on c_1 and c_2 in the form $n^T(c_1 - c_2 - v) \ge 0$ for some vector $n \in \mathbb{R}^3$.

The points u and v can be computed by using standard optimization algorithms. Some results are shown in Fig. 4. In each case, Δa is marked with a star, and Δb with a diamond. The three plots correspond to the cases when v is on a sharp edge, the top, and the side surface of the cylinder, respectively.

Δa and Δb Are Not Visible to Each Other

Let p and q be the entry point and the exit point of a shortest curve in $\mathbb{R}^3 \backslash W$ from Δa to Δb as defined after Proposition 3.

Because Δa is in the interior of $\mathbb{R}^3 \backslash W$ by assumption, p is located on the contour of W with respect to a viewer situated at Δa. Among all of the planes that are tangent to ∂W at p, let P_a be the one that passes through Δa. The choice of P_a is unique unless p is on

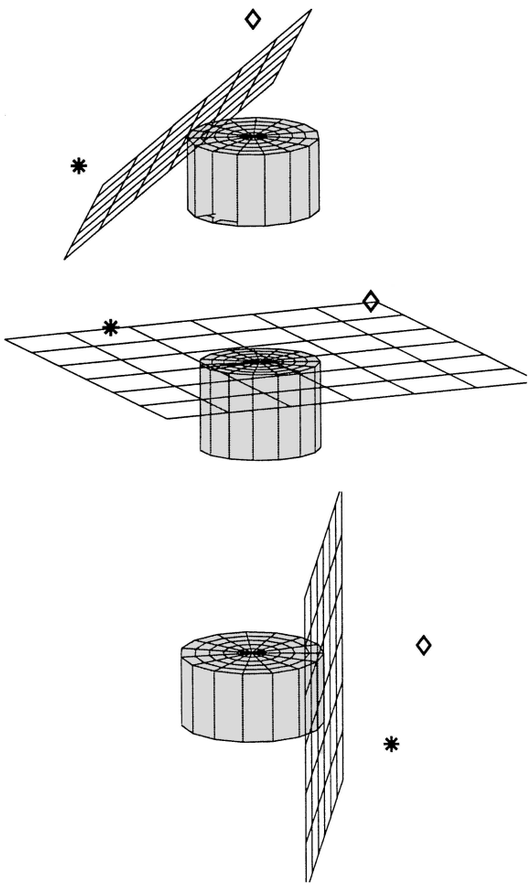

Fig. 4 Approximated feasible region for Δc when Δa and Δb are visible to each other.

the sharp edges of ∂W and Δa has the same z coordinate as p. In the latter case, we can choose an arbitrary tangent plane. Let P_a^+ be the closed half-space determined by the side of P_a that does not contain W. Points in P_a^+ are visible to Δa. In a similar way, we can define P_b^+ based on the tangent plane P_b to ∂W at q that passes through Δb. Points in P_b^+ are visible to Δb. Therefore, points in $P^+ \triangleq P_a^+ \cap P_b^+$ are visible to both Δa and Δb and can be used as the approximated feasible set of Δc. This translates into two linear constraints on c_1 and c_2.

Some typical examples are plotted in Fig. 5, where, in each case, Δa is marked with a star and Δb a diamond, and the solid line is a shortest curve in $\mathbb{R}^3 \backslash W$ connecting Δa and Δb .

In summary, given Δa and Δb, one or two linear inequalities can be used to approximate the constraint that Δc is visible to both Δa and Δb in the presence of the obstacle W. Such a linear approximation should be carried out for all aircraft pairs, thus leading to the following approximated version of problem (16):

$$\text{Minimize} \quad \sum_{i=1}^{n} \mu_i \left\| c_i - c_i^u \right\|^2 \quad \text{subject to} \quad c_i - c_j \in P_{ij}^+ \qquad 1 \le i < j \le n \quad (17)$$

where P_{ij}^+ is the linear approximation of the feasible set for $c_i - c_j$ computed based on $a_i - a_j$ and $b_i - b_j$, as described earlier. Problem (17) is a linearly constrained quadratic programming problem that can be efficiently solved by many existing software packages.

Some Examples of Multiaircraft Encounters

Consider a three-aircraft encounter where $a_1 = (0, 50, 4)$, $b_1 = (100, 50, 4)$, $a_2 = (50, 0, 4)$, $b_2 = (50, 100, 4)$, $a_3 = (100, 100, 5)$, and $b_3 = (0, 0, 3)$, that is, where aircraft 1 and aircraft 2 are flying at the same altitude with cross-path angle of 90 deg, whereas aircraft 3 dives across that altitude and has a path angle of 135 deg with both aircraft 1 and aircraft 2. All three aircraft have the same priority, and $t_c = (t_0 + t_f)/2$. We choose a larger $R (R = 10$ n mile) to make the resolution maneuvers evident. H is chosen to be 0.3292 n mile. In Fig. 6, the solutions to problem (17) corresponding to two different values of η are shown. Plotted in Fig. 6a is the snapshot at a time instant near t_c of the two-legged joint maneuver that is a solution to problem (17) with $\eta = 5$. Its top view is shown in Fig. 6b. The cylinders in Fig. 6a represent half of the size of the protection zones surrounding the aircraft, that is, they are (open) cylinders of radius $R/2$ and height H. Therefore, two aircraft are in a conflict situation if and only if the corresponding cylinders intersect each other. Similarly, Figs. 6c and 6d plot a snapshot of a solution to problem (17) with $\eta = 50$. As in the case of two-aircraft encounters, a larger value of η will force the aircraft to adopt horizontal maneuvers to resolve the conflict.

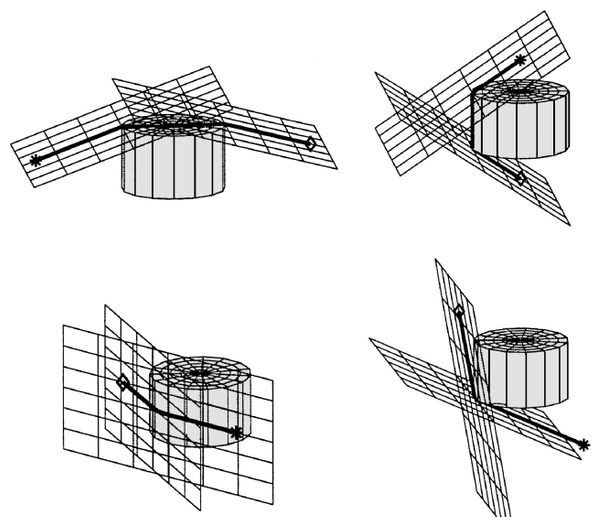

Fig. 5 Approximated feasible region for Δc when Δa and Δb are not visible to each other.

Figure 7 shows the simulation results for a four-aircraft encounter with $a_1 = (0, 100, 4)$, $b_1 = (100, 0, 4)$, $a_2 = (20, 80, 4)$, $b_2 = (80, 20, 4)$, $a_3 = (95, 95, 4)$, $b_3 = (0, 0, 4)$, $a_4 = (70, 65, 4)$, and $b_4 = (20, 25, 4)$. The four aircraft are divided into two groups, each consisting of two aircraft, one overtaking the other, with the path angle between the two groups being 90 deg. We choose $R = 10$ n mile, $H = 0.3292$ n mile, and $t_c = (t_0 + t_f)/2$. All aircraft have equal priority. Figures 7a and 7b plot the snapshot of a solution at a time instant near t_c when $\eta = 5$. Figures 7c and 7d plot a snapshot of a solution when $\eta = 50$. Figures 7c and 7d can be thought of as the restricted solution to problem (17) when the motion of each aircraft is required to be contained in the plane of altitude 4. If we increase the priority of aircraft 1 such that $\mu_1 = 0.7$ and $\mu_2 = \mu_3 = \mu_4 = 0.1$, we obtain the results shown in Figs. 8a and 8b for $\eta = 5$ and 50, respectively. Compared with Figs. 7a and 7d, the motions of aircraft 1 (shown in Fig. 8 by the heavy lines) are closer to the straight line motions, forcing other aircraft to bend more.

As the number of aircraft involved gets larger, the resolution maneuver becomes more complicated. An example is shown in Fig. 9 for an eight-aircraft encounter, which is obtained by adding to the four-aircraft encounter in Figs. 7 and 8 four more aircraft with $a_5 = (55, 0, 3.7)$, $b_5 = (50, 80, 3.7)$, $a_6 = (55, 20, 3.7)$, $b_6 = (50, 100, 3.7)$, $a_7 = (0, 55, 3.7)$, $b_7 = (80, 45, 4)$, $a_8 = (20, 55, 3.7)$, and $b_8 = (100, 45, 4)$. By choosing identical priority and $\eta = 20$, the obtained solution to problem (17) consists of both horizontal and vertical resolution motions. Figures 9a–9c are views of the solution from different viewpoints. Figure 9d is its snapshot at a certain time instant.

In each simulation, a large portion of the computational time is spent on linearizing the feasible region, which is very sensitive to the configuration of the starting and destination positions of the aircraft.

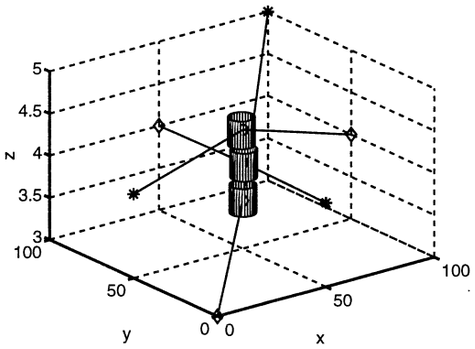

a) Three-dimensional representation

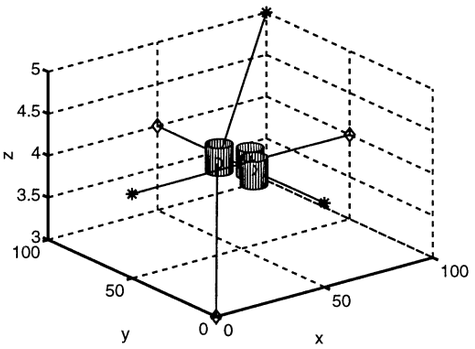

c) Three-dimensional representation

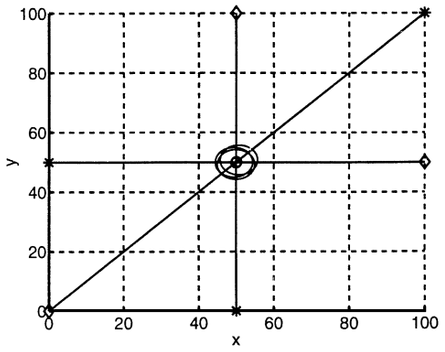

b) Top view (case $\eta = 5$)

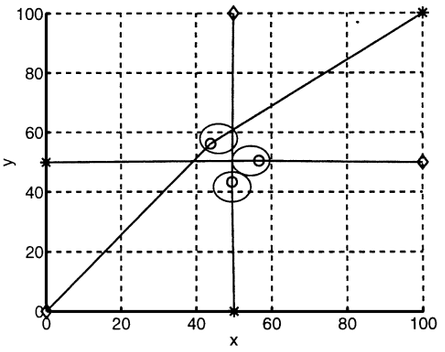

d) Top view (case $\eta = 50$)

Fig. 6 Two-legged resolution maneuvers for a three-aircraft encounter ($\mu_1 = \mu_2 = \mu_3 = \frac{1}{3}$).

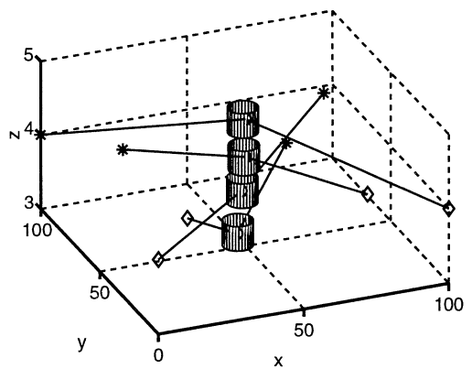

a) Three-dimensional representation

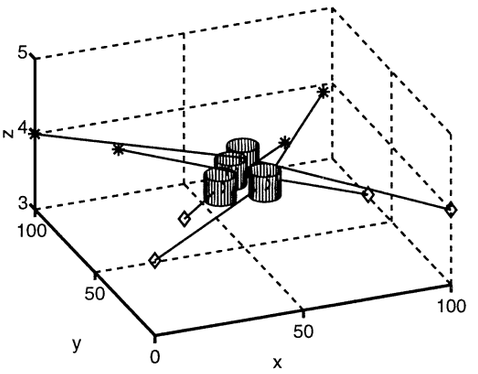

c) Three-dimensional representation

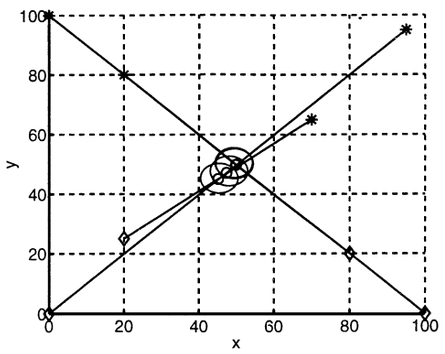

b) Top view (case $\eta = 5$)

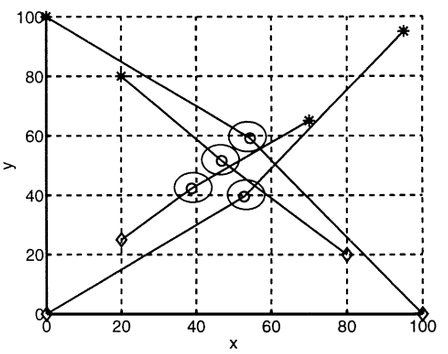

d) Top view (case $\eta = 50$)

Fig. 7 Two-legged resolution maneuvers for a four-aircraft encounter ($\mu_1 = \mu_2 = \mu_3 = \mu_4 = \frac{1}{4}$).

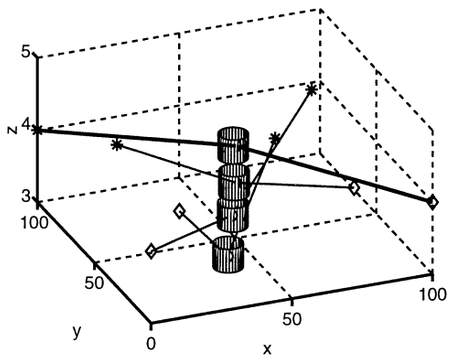

a) Three-dimensional representation (case $\eta = 5$)

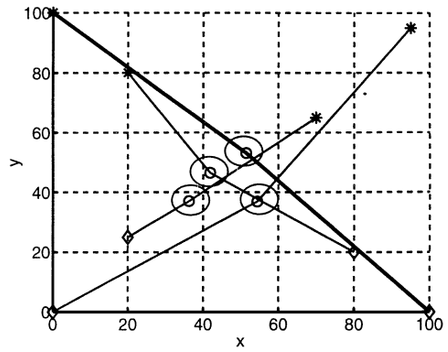

b) Top view (case $\eta = 50$)

Fig. 8 Two-legged resolution maneuvers for the four-aircraft encounter ($\mu_1 = 0.7$ and $\mu_2 = \mu_3 = \mu_4 = 0.1$).

On a desktop personal computer with 450-MHz Pentium III processor, the computational time for the 3-, 4-, and 8-aircraft examples (implemented in MATLAB®) is 4.7500, 3.9370, and 26.1720 s, respectively. These times could be significantly reduced by writing the code in programming languages more efficient than MATLAB, thus making the algorithm suitable for real-time implementations.

Further Constraints on the Waypoints for the Maneuver Feasibility

Thus far we have assumed that the two-legged maneuver obtained by solving the optimization problem (17) is flyable. In practice, this is usually not the case because of the abrupt turn and the change of speed when an aircraft passes through its waypoint. In the following, we shall propose practical constraints on the waypoints to alleviate such drawbacks, at least to a certain extent. For the optimization problem to be computationally tractable, it is important that the introduced constraints are convex.

We start by considering the speed constraint. Suppose that the speed of each aircraft during both stages of its maneuver cannot exceed a certain threshold $v_{\max}$. Recall that t_c is the time epoch corresponding to the middle waypoints. Then the speed constraint can be expressed as

$$\|a_i - c_i\| \le v_{\max}(t_c - t_0), \qquad \|b_i - c_i\| \le v_{\max}(t_f - t_c) \qquad i = 1, \ldots, n \quad (18)$$

For a single aircraft i, constraint (18) implies that c_i must belong to the intersection of two balls, one centered at a_i and the other centered at b_i. Hence, the speed constraint is convex. Instead of a common $v_{\max}$, one can also impose different speed upper bounds for different aircraft in the two stages.

A further practical constraint is the turning angle constraint. Suppose that the angle each aircraft turns at a waypoint cannot exceed a certain threshold $\theta_{\max}$. For aircraft i, this constraint specifies that its waypoint c_i must lie in a convex region of $\mathbb{R}^3$ that is invariant under rotations around the axis $\overline{a_i b_i}$, where $\overline{a_i b_i}$ denotes the straight

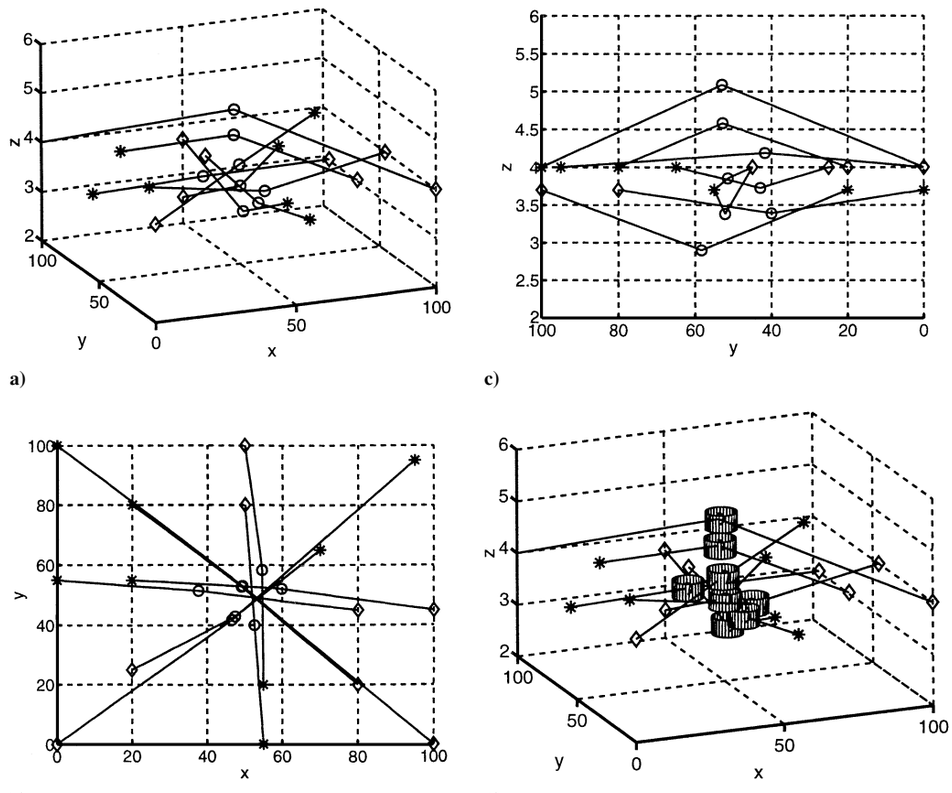

Fig. 9 Two-legged resolution maneuver for an eight-aircraft encounter ($\mu_i = \frac{1}{8}$, $i = 1, \ldots, 8$, and $\eta = 20$).

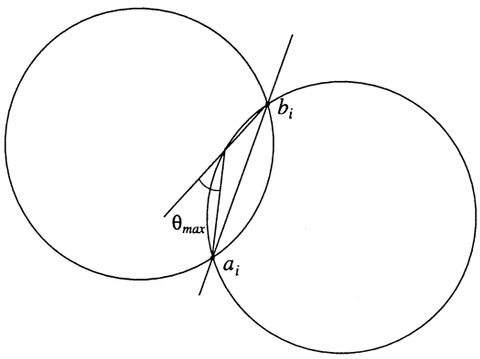

Fig. 10 Turning angle constraint on waypoints.

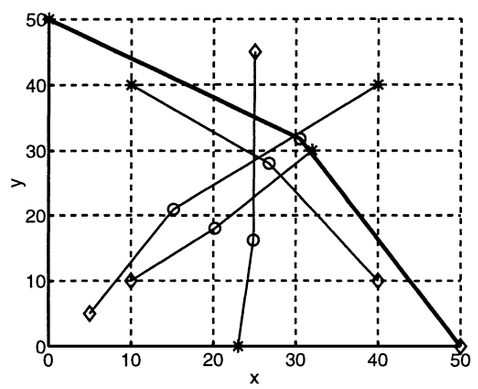

a) No additional constraint

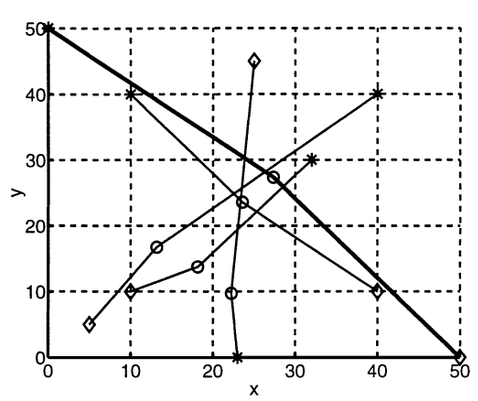

b) Speed constraint with $v_{\max} = 7.102$ n mile/min

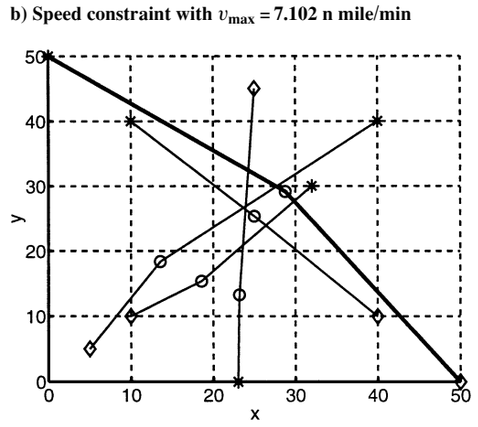

c) Turning angle constraint with $\theta_{\max} = \pi/10$

Fig. 11 Two-legged resolution maneuvers for a five-aircraft encounter ($\mu_1 = \mu_2 = \mu_3 = \mu_4 = \mu_5 = \frac{1}{5}$ and $\eta = 50$).

line passing through a_i and b_i. The intersection of this convex region with any plane through $\overline{a_i b_i}$ is plotted in Fig. 10. It is the intersection of two disks with properly chosen centers and radii.

Note that each of the two preceding constraints can be expressed as a second-order cone constraint of the form (assume s is the optimization variable)

$$\|\hat{A}s + \hat{\boldsymbol{b}}\| \leq \hat{\boldsymbol{c}}s + \hat{d} \tag{19}$$

for some matrix $\hat{A}$, vectors $\hat{\boldsymbol{b}}$ and $\hat{\boldsymbol{c}}$, and constant $\hat{d}$, of suitable dimensions. Although the turning angle constraint is actually equivalent to an infinite number of second-order cone constraints, one can, for example, impose upper bounds on the turning angles for the projections of the maneuver onto the plane xy, xz, and yz, respectively, thus leading to three second-order cone constraints. Therefore, the optimization problem (17), together with the speed and the simplified turning angle constraints, becomes a second-order cone programming (SOCP) problem, which can be solved by using software such as SOCP.[28] Note that, as before, the vertical penalty factor η can be incorporated into these two constraints.

Figure 11 shows the effect of the speed and the turning angle constraints by considering a five-aircraft encounter. Here we choose $t_0 = 0$ min, $t_f = 10$ min, $t_c = 5$ min, $\eta = 50$, $R = 5$ n mile, $H = 0.3292$ n mile, and we assign the same priority to all of the aircraft. The solution to problem (17) without any additional constraint is shown in Fig. 11a, the solution with the speed constraint of $v_{\max} = 7.102$ n mile/min is shown in Fig. 11b, whereas the solution with the turning angle constraint $\theta_{\max} = \pi/10$ on the xy plane projection is plotted in Fig. 11c. As expected, the aircraft that possesses the largest speed and turning angle in Fig. 11a (whose trajectory is highlighted by a heavy line) tends to have a straighter and smoother motion under the additional constraints on either the speed or the turning angle.

Further adjustments can be introduced to improve the flyability of the generated maneuvers. For example, one can consider multilegged maneuvers and adopt an iterative procedure to get an approximated optimal solution for the multilegged version of the conflict resolution problem. Furthermore, to avoid sharp turns at time t_0, one can choose the starting epoch to be $t_0 + \Delta$ for some positive Δ and use the time interval $[t_0, t_0 + \Delta]$ as a buffer for possible heading adjustments. Much more work is still needed in this regard to actually implement our algorithms in practical situations.

Conclusions

In this paper, the problem of designing optimal conflict-free maneuvers for multiple-aircraft encounters in three-dimensional airspace is studied. Numerical algorithms for solving the problem are introduced based on a simplified model of the aircraft dynamics, and their effectiveness is shown by extensive simulations. The proposed algorithms rest on a geometric interpretation of the solutions and possess some features that make them attractive for practical implementation. For example, aircraft may have different priorities, vertical maneuvers are penalized, and the maximum speed and turning angle constraints can be introduced to improve path flyability. This paper represents a step toward the implementation of an effective optimal conflict resolution algorithm in practical situations.

Appendix: Numerical Procedure to Solve Problem (10)

We describe a numerical procedure to solve problem (10) in each one of the three cases enumerated at the end of the section "Shortest Curve Between Two Points in $\mathbb{R}^3$ Avoiding a Cylindrical Obstacle."

Case 1

By the symmetry of D, we consider only the case when both $a = (a_x, a_y, a_z)$ and $b = (b_x, b_y, b_z)$ are outside of Q and $|a_z| \leq h$; the case when $|b_z| \leq h$ is similar. Without loss of generality we can assume that $a_y = 0$, $a_x \leq -r$, and $b_y \geq 0$. To find a shortest curve in $\mathbb{R}^3 \backslash D$ between a and b, we need to focus only on those curves contained in $\{(x, y, z) : y \geq 0\}$. Specifically, solutions to problem (10) may have the following possible configurations: 1) LS_TL, a line segment from a to $p \in \partial D_T \cap \partial D_S$ followed by a line segment from p to b; 2) LS_TLS_TL, a line segment from a to $p \in \partial D_T \cap \partial D_S$, then a line segment from p to $q \in \partial D_T \cap \partial D_S$

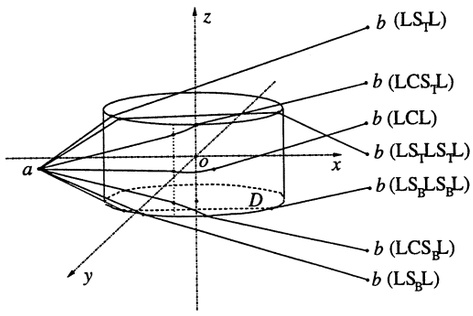

a) Case 1

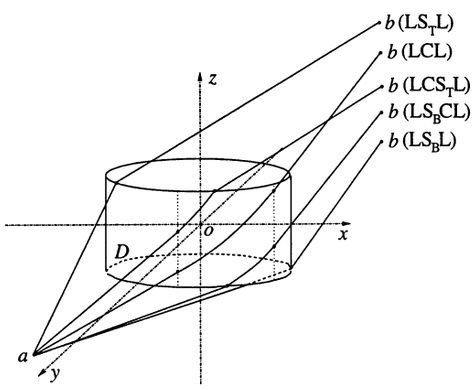

b) Case 2

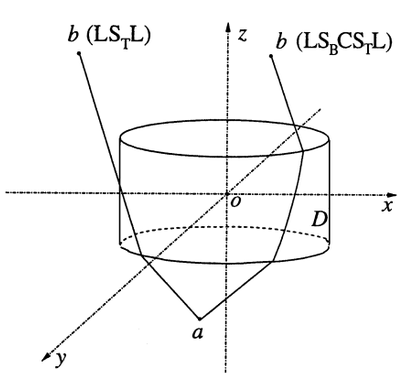

c) Case 3

Fig. A1 Possible configurations for the solutions.

in ∂D_T, and finally a line segment from q to b; 3) LCS_TL, a line segment from a to $p \in \partial D_S$, then a helix on ∂D_S from p to $q \in \partial D_T \cap \partial D_S$, and finally a line segment from q to b; 4) LCL, a line segment from a to $p \in \partial D_S$, followed by a helix from p to $q \in \partial D_S$, and finally a line segment from q to b; 5) LCS_BL, a mirror image of configuration LCS_TL across the xy plane, that is, a line segment from a to $p \in \partial D_S$, then a helix on ∂D_S from p to $q \in \partial D_B \cap \partial D_S$, and finally a line segment from q to b; 6) LS_BLS_BL, a mirror image of configuration LS_TLS_TL across the xy plane; and 7) LS_BL, a mirror image of configuration LS_TL across the xy plane.

See Fig. A1a for the plots of these configurations. In some degenerate cases, one solution may belong to two configurations at the same time.

Depending on the specific position of b, only a subset of the configurations should be considered. For example, if b has z coordinate $b_z > h$, then only configurations LS_TL, LCS_TL, and LCL are possible. If $|b_z| \le h$, then possible configurations are LS_TLS_TL, LCL, and LS_BLS_BL. If $b_z < -h$, then only configurations LS_BL, LCS_BL, and LCL should be considered.

Given a and b, we can find a shortest curve in each one of the possible configurations. A global solution is the shortest one of them. We now show how to compute a shortest curve for some typical configurations.

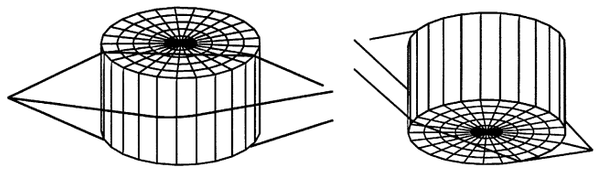

Fig. A2 Three configurations of case 1 viewed from two different angles ($r = 5$ and $h = 3$).

Consider the case when $b_z > h$. The optimal entry point p in configuration LS_TL can be obtained by solving the following optimization problem:

$$\text{Minimize} \quad \|a - (r\cos\theta, r\sin\theta, h)\| + \|b - (r\cos\theta, r\sin\theta, h)\| \tag{A1}$$

for θ subject to the constraint that $(r\cos\theta, r\sin\theta, h)$ is visible to a, which translates into $\theta \in [\theta_-, \theta_+]$ for some θ_- and θ_+ with $\theta_- \le \theta_+$. This optimization problem can be solved by many standard numerical algorithms efficiently. In most practical situations, the existence of local minima is not a problem because the cost function (A1) either has a unique interior minimum, or has a minimum at the boundary θ_- or θ_+, which is a hint that the corresponding neighboring configuration can provide even better solutions. This phenomenon is typical for other configurations as well.

Another possible configuration when $b_z > h$ is LCS_TL. In this case, denote $p = (r\cos\theta_0, r\sin\theta_0, z)$ for some $z \in [-h, h]$, where θ_0 is determined by the contour of D for a viewer sitting at a (shown in Fig. A1a by the vertical dotted line), and let $q = (r\cos\theta, r\sin\theta, h)$ for some θ such that q is visible to b and $|\theta - \theta_0| \le \pi$. Then the optimal p and q are obtained by solving the following problem:

$$\text{Minimize} \quad \|a - (r\cos\theta_0, r\sin\theta_0, z)\| + \sqrt{(h-z)^2 + r^2(\theta_0 - \theta)^2} + \|b - (r\cos\theta, r\sin\theta, h)\|$$

Note that the feasible region of (z, θ) is a compact rectangle, thus, the preceding optimization problem admits a solution that can be computed by using, for example, the fminsearch function in MATLAB.

Other configurations can be solved similarly. Note that configuration LCL is the only one for which an analytic solution exists and can be obtained by a simple geometric construction (unwrapping the cylinder).

Shortest curves assuming different configurations in case 1 are shown in Fig. A2 with one endpoint fixed and the other one assuming various positions.

Case 2

We now study the case when both $a = (a_x, a_y, a_z)$ and $b = (b_x, b_y, b_z)$ are outside of Q and neither of them has z coordinate in $[-h, h]$. Because a and b are supposed to be invisible to each other, one of them has z coordinate smaller than $-h$, and the other has z coordinate greater than h. We assume without loss of generality that $a_z < -h$ and $b_z > h$. As in case 1, we assume that the coordinate axes are properly chosen such that $a_y = 0$, $a_x \le -r$, and $b_y \ge 0$, so that we can focus on the curves contained in $\{(x, y, z) : y \ge 0\}$.

The five possible configurations for a shortest curve in $\mathbb{R}^3 \backslash D$ connecting a and b are plotted in Fig. A1b. They include three configurations LS_TL, LCS_TL, and LCL already introduced in case 1, and two new configurations, LS_BCL and LS_BL. Configuration LS_BCL consists of first a line segment from a to $p \in \partial D_B \cap \partial D_S$, then a helix on ∂D_S from p to $q \in \partial D_S$, and finally a line segment from q to b. Configuration LS_BL consists of two line segments with a turning point belonging to $\partial D_B \cap \partial D_S$. The process of obtaining a shortest curve joining a and b for each configuration is entirely analogous to case 1; hence, it is omitted.

Case 3

Finally, consider the case when at least one of a and b (for example, a) belongs to Q. By a possible reflection across the xy

plane, we assume $a_z \leq -h$. Then, depending on the location of b, there are two possible configurations for a shortest curve in $\mathbb{R}^3 \backslash D$ between a and b, which are plotted in Fig. A1c: 1) LS_BL, two line segments with a turning point at $p = q \in \partial D_B \cap \partial D_S$, and 2) LS_BCS_TL, a helix on ∂D_S sandwiched by two line segments such that $p \in \partial D_B \cap \partial D_S$ and $q \in \partial D_T \cap \partial D_S$.

If b belongs to Q, then only configuration LS_BCS_TL is possible. Otherwise, both of the two configurations have to be considered. A shortest curve in each configuration is obtained in the same way as before. However, note here that for configuration LS_BCS_TL, unlike the preceding cases, the existence of local minima does pose some problems because the optimization is over the product of two circles $\partial D_T \cap \partial D_S$ and $\partial D_B \cap \partial D_S$, that is, a torus. We suggest partitioning each of the two circles into several segments, solving the optimization problem in each segment, and then choosing the best one. We shall not go into further details because they are irrelevant to the main development.

Acknowledgments

This research has been supported by the Defense Advanced Research Projects Agency (DARPA) under Contract F33615-98-C-3614, by the National Science Foundation Knowledge and Distributed Intelligence (KDI) 9873474, by the project "Sensor Webs of SmartDust: Distributed Processing/Data Fusion/Inferencing in Large Microsensor Arrays" under DARPA Contract F30602-00-2-0538, and by the project "New Techniques for the Identification and Adaptive Control of Industrial Systems" funded by the Italian Ministry of Education, University, and Research. The authors would like to thank Arnab Nilim for his help with the simulations and to acknowledge the anonymous reviewers for their useful comments.

References

[1]Kuchar, J. K., and Yang, L. C., "A Review of Conflict Detection and Resolution Modeling Methods," *IEEE Transactions on Intelligent Transportation Systems*, Special Issue on Air Traffic Control—Part I, Vol. 1, No. 4, 2000, pp. 179–189.

[2]Pappas, G. J., Tomlin, C., Lygeros, J., Godbole, D., and Sastry, S., "A Next Generation Architecture for Air Traffic Management Systems," *Proceedings of the 36th IEEE Conference on Decision and Control*, Vol. 3, IEEE Publ., Piscataway, NJ, 1997, pp. 2405–2410.

[3]Tomlin, C., Lygeros, J., and Sastry, S., "A Game Theoretic Approach to Controller Design for Hybrid Systems," *Proceedings of the IEEE*, Vol. 88, No. 7, 2000, pp. 949–970.

[4]Tomlin, C., Pappas, G. J., and Sastry, S., "Conflict Resolution for Air Traffic Management: A Study in Multi-Agent Hybrid Systems," *IEEE Transactions on Automatic Control*, Vol. 43, No. 4, 1998, pp. 509–521.

[5]Teo, R., and Tomlin, C., "Computing Provably Safe Aircraft to Aircraft Spacing for Closely Spaced Parallel Approaches," *Proceedings of the 19th Digital Avionics Systems Conference (DASC00)*, Vol. 1, IEEE Publ., Piscataway, NJ, 2000, pp. 2D2/1–9.

[6]Medioni, F., Durand, N., and Alliot, J. M., "Air Traffic Conflict Resolution by Genetic Algorithms," *Artificial Evolution, European Conference (AE 95)*, Springer-Verlag, Berlin, 1995, pp. 370–383.

[7]Frazzoli, E., Mao, Z.-H., Oh, J.-H., and Feron, E., "Resolution of Conflicts Involving Many Aircraft via Semidefinite Programming," *Journal of Guidance, Control, and Dynamics*, Vol. 24, No. 1, 2001, pp. 79–86.

[8]Hu, J., Prandini, M., and Sastry, S., "Optimal Maneuver for Multiple Aircraft Conflict Resolution: A Braid Point of View," *Proceedings of the 39th IEEE Conference on Decision and Control*, Vol. 4, IEEE Publ., Piscataway, NJ, 2000, pp. 4164–4169.

[9]Menon, P. K., Sweriduk, G. D., and Sridhar, B., "Optimal Strategies for Free-Flight Air Traffic Conflict Resolution," *Journal of Guidance, Control, and Dynamics*, Vol. 22, No. 2, 1999, pp. 202–211.

[10]Zhao, Y., and Schultz, R., "Deterministic Resolution of Two Aircraft Conflict in Free Flight," *Proceedings of AIAA Guidance, Navigation, and Control Conference*, AIAA, Reston, VA, 1997, pp. 469–478.

[11]Paielli, R. A., and Erzberger, H., "Conflict Probability Estimation for Free Flight," *Journal of Guidance, Control, and Dynamics*, Vol. 20, No. 3, 1997, pp. 588–596.

[12]Krozel, J., and Peters, M., "Strategic Conflict Detection and Resolution for Free Flight," *Proceedings of the 36th IEEE Conference on Decision and Control*, Vol. 2, IEEE Publ., Piscataway, NJ, 1997, pp. 1822–1828.

[13]Hu, J., Lygeros, J., Prandini, M., and Sastry, S., "Aircraft Conflict Prediction and Resolution Using Brownian Motion," *Proceedings of the 38th IEEE Conference on Decision and Control*, Vol. 3, IEEE Publ., Piscataway, NJ, 1999, pp. 2438–2443.

[14]Prandini, M., Hu, J., Lygeros, J., and Sastry, S., "A Probabilistic Approach to Aircraft Conflict Detection," *IEEE Transactions on Intelligent Transportation Systems*, Special Issue on Air Traffic Control—Part I, Vol. 1, No. 4, 2000, pp. 199–220.

[15]Krozel, J., and Peters, M., "Conflict Detection and Resolution for Free Flight," *Air Traffic Control Quarterly*, Vol. 5, No. 3, 1997, pp. 181–212.

[16]Lygeros, J., and Lynch, N., "On the Formal Verification of the TCAS Conflict Resolution Algorithms," *Proceedings of the 36th IEEE Conference on Decision and Control*, Vol. 2, IEEE Publ., Piscataway, NJ, 1997, pp. 1829–1834.

[17]Radio Technical Commission for Aeronautics (RTCA), "Minimum Operational Performance Standards for Traffic Alert and Collision Avoidance System II (TCAS II) Airborne Equipment," RTCA, Inc., TR RTCA/DO-185A, Washington, DC, Dec. 1997.

[18]Kosecka, J., Tomlin, C., Pappas, G. J., and Sastry, S., "Generation of Conflict Resolution Maneuvers for Air Traffic Management," *Proceedings of the 1997 IEEE International Conference on Intelligent Robot and Systems. Innovative Robotics for Real-World Applications, IROS'97*, Vol. 3, IEEE Publ., Piscataway, NJ, 1997, pp. 1598–1603.

[19]Bicchi, A., and Pallottino, L., "On Optimal Cooperative Conflict Resolution for Air Traffic Management Systems," *IEEE Transactions on Intelligent Transportation Systems*, Special Issue on Air Traffic Control—Part I, Vol. 1, No. 4, 2000, pp. 221–231.

[20]Niedringhaus, W. P., "Stream Option Manager (SOM): Automated Integration of Aircraft Separation, Merging, Stream Management, and Other Air Traffic Control Functions," *IEEE Transactions on Systems, Man, and Cybernetics*, Vol. 25, No. 9, 1995, pp. 1269–1280.

[21]Hu, J., Prandini, M., and Sastry, S., "Optimal Coordinated Maneuvers for Multiple Agents Moving on a Plane," *SIAM Journal on Control and Optimization* (submitted for publication).

[22]Chen, Y.-B., Hsieh, M., Inselberg, A., and Lee, H. Q., "Planar Conflict Resolution for Air Traffic Control," *Proceedings of the Second Canadian Conference on Computational Geometry*, Univ. of Ottawa, Ottawa, 1990, pp. 160–163.

[23]Inselberg, A., "Conflict Resolution, One-Shot Problem, and Air Traffic Control," *Abstracts of the First Canadian Conference on Computional Geometry*, McGill Univ., Montreal, 1989, p. 26.

[24]Chiang, Y.-J., Klosowski, J. T., Lee, C., and Mitchell, J. S. B., "Geometric Algorithms for Conflict Detection/Resolution in Air Traffic Management," *Proceedings of the 36th IEEE Conference on Decision and Control*, Vol. 2, IEEE Publ., Piscataway, NJ, 1997, pp. 1835–1840.

[25]Milnor, J., *Morse Theory*, Princeton Univ. Press, Princeton, NJ, 1963, pp. 70–74.

[26]Mitchell, J. S. B., "Shortest Paths and Networks," *CRC Handbook of Discrete and Computational Geometry*, edited by J. E. Goodman and J. O'Rourke, CRC Press, Boca Raton, FL, 1997, pp. 445–466.

[27]Mitchell, J. S. B., "Geometric Shortest Paths and Network Optimization," *Handbook of Computational Geometry*, edited by J.-R. Sack and J. Urrutia, North-Holland, Amsterdam, 2000, pp. 633–701.

[28]Lobo, M., Vandenberghe, L., Boyd, S., and Lebret, H., "Applications of Second-Order Cone Programming," *Linear Algebra and Its Applications*, Vol. 284, No 1–3, 1998, pp. 193–228.